
Drifting Fields are not Conservative

Leonard Franz *

Eberhard Karls Universität Tübingen
leonard.tobias-franz@uni-tuebingen.de

Sebastian Hoffmann *

Max Planck Institute for Biogeochemistry
Eberhard Karls Universität Tübingen
shoffmann@bgc-jena.mpg.de

Georg Martius

Eberhard Karls Universität Tübingen
georg.martius@uni-tuebingen.de

Abstract

Drifting models generate high-quality samples in a single forward pass by transporting generated samples toward the data distribution using a vector valued drift field. We investigate whether this procedure is equivalent to optimizing a scalar loss and find that, in general, it is not: drift fields are *not conservative*—they cannot be written as the gradient of any scalar potential. We identify the position-dependent normalization as the source of non-conservatism. The Gaussian kernel is the unique exception where the normalization is harmless and the drift field is exactly the gradient of a scalar function. Generalizing this, we propose an alternative normalization via a related kernel (the sharp kernel) which restores conservatism for any radial kernel, yielding well-defined loss functions for training drifting models. While we identify that the drifting field matching objective is strictly more general than loss minimization, as it can implement non-conservative transport fields that no scalar loss can reproduce, we observe that practical gains obtained utilizing this flexibility are minimal. We thus propose to train drifting models with the conceptually simpler formulations utilizing loss functions.

1 Introduction

Generative modeling via *drifting* [Deng et al., 2026] has recently attracted considerable attention due to its high sample quality and fast one-step inference. Their model training framework formalizes training as repeatedly moving generated samples toward the data distribution via a so-called “drift field” and then updating parameters so that the model reproduces this movement. This is remarkably different from most of machine learning, where training is formulated as the optimization of scalar fields (the loss). This raises a natural question: is drifting implicitly optimizing a loss function, and if so, what is the corresponding objective?

To make this notion more precise, consider the loss used in the drifting formalism for inducing the sample transport:

$$\mathcal{L}^{\text{drift}}(\theta) = \mathbb{E}_{\varepsilon} [\|f_{\theta}(\varepsilon) - \text{sg}(f_{\theta}(\varepsilon) + \mathbf{V}_{p,q_{\theta}}(f_{\theta}(\varepsilon)))\|^2], \quad (1)$$

where $f_{\theta} : \mathbb{R}^n \rightarrow \mathbb{R}^n$ is the generator, $\mathbf{V}_{p,q_{\theta}} : \mathbb{R}^n \rightarrow \mathbb{R}^n$ is the vector valued drift field, and sg denotes the stop-gradient operator. We observe that Equation (1), which we call the “stop-gradient objective”, can implement *any* transport field $\mathbf{V} : \mathbb{R}^n \rightarrow \mathbb{R}^n$ for the generated outputs $f_{\theta}(\varepsilon)$, including non-conservative ones. That includes curling fields and fields that induce non-converging transport in closed loops. On the contrary, transport fields induced when optimizing a scalar field via $\nabla_{\theta} \mathcal{L}(f_{\theta})$ are by definition conservative, making Equation (1) strictly more general.

*Equal contribution.

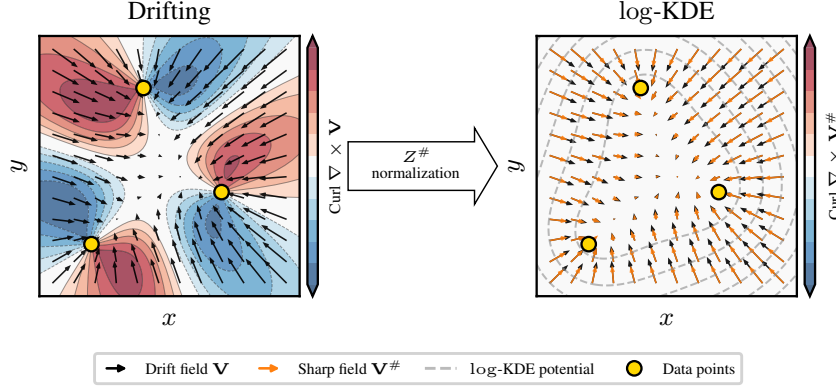


Figure 1: Drifting fields are generally not conservative, as seen by the non-vanishing curl of the drifting field in the case of a Laplacian kernel (left). We propose a new normalization $Z^\#$ of the drifting field via the *sharp kernel* kernel density estimate (KDE) that leaves field direction unchanged while restoring the fields conservatism (right). This allows us to reformulate the drifting field as the gradient of a scalar potential – the log-KDE potential – yielding a simplified objective and a interpretable decreasing metric measuring training progress.

Deng et al. investigate the connection to loss-based optimization by relating the gradient of the squared MMD loss [Gretton et al., 2006] to the drifting field. They find that the induced transport shares the same direction as the drift field but lacks position-dependent normalization and that directly optimizing the MMD does not work in practice. They argue that the advantage of the drifting framework lies precisely in the stop-gradient’s extra generality, as it allows them to incorporate position-dependent normalization—something that, they imply, no scalar loss can reproduce.

We show that this claim is both correct and overstated. It is correct in the sense that the specific normalization used by Deng et al. is indeed not reproducible by any loss: for most kernel choices, the drift field is *not conservative*—its Jacobian is not symmetric, and no scalar potential exists whose gradient recovers it. However, the claim is overstated because loss-based training with normalization *is* possible—just with a different normalization. We introduce the *sharp kernel* $k^\#$, which, when used in place of the kernel k in the normalization, yields a conservative field with a potential given by a “naive KL divergence” between KDEs built from the sharp kernel.

Our experiments confirm that sharp normalization performs comparably to the original drift field, suggesting that the non-conservative component—the very part that requires the stop-gradient’s extra generality—does not contribute to performance. Moreover, sharp normalization yields improved tail behavior in the case of the Laplacian kernel, where, unlike for the original drift field which grows without bound far from the data, remains of constant magnitude.

The reformulation of drifting model training with a scalar potential allows us to simplify the implementation and removes the requirement to explicitly construct a sample transport field \mathbf{V} .

2 Background

Drifting Models A generator network $f_\theta : \mathbb{R}^C \rightarrow \mathbb{R}^D$ maps noise $\varepsilon \sim p_\varepsilon$ to samples $\mathbf{x} = f_\theta(\varepsilon)$, inducing a pushforward distribution $q_\theta = (f_\theta)_\# p_\varepsilon$. Drifting models [Deng et al., 2026] evolve q_θ during training via a *drift field* $\mathbf{V}_{p,q} : \mathbb{R}^D \rightarrow \mathbb{R}^D$ that transports generated samples toward the data distribution p :

$$\mathbf{x}_{i+1} = \mathbf{x}_i + \mathbf{V}_{p,q_i}(\mathbf{x}_i). \quad (2)$$

The drift field is constructed from an attractive component \mathbf{V}_p^+ pulling toward data samples and a repulsive component \mathbf{V}_q^- pushing away from generated samples:

$$\mathbf{V}_{p,q}^{\text{drift}}[k](\mathbf{x}) := \underbrace{\frac{1}{Z_p(\mathbf{x})} \mathbb{E}_{\mathbf{y}^+ \sim p}[k(\mathbf{x}, \mathbf{y}^+)(\mathbf{y}^+ - \mathbf{x})]}_{:= \mathbf{V}_p^+ \text{ drift}} - \underbrace{\frac{1}{Z_q(\mathbf{x})} \mathbb{E}_{\mathbf{y}^- \sim q}[k(\mathbf{x}, \mathbf{y}^-)(\mathbf{y}^- - \mathbf{x})]}_{:= \mathbf{V}_q^- \text{ drift}} \quad (3)$$

where k is a kernel function and $Z_p(\mathbf{x}) := \mathbb{E}_{\mathbf{y}^+ \sim p}[k(\mathbf{x}, \mathbf{y}^+)]$, $Z_q(\mathbf{x}) := \mathbb{E}_{\mathbf{y}^- \sim q}[k(\mathbf{x}, \mathbf{y}^-)]$ are normalization factors. By construction, $\mathbf{V}_{p,q}$ is anti-symmetric ($\mathbf{V}_{p,q} = -\mathbf{V}_{q,p}$) and vanishes when $q = p$.

Deng et al. [2026] formulate training as a fixed-point iteration: at step i , the network should satisfy $f_{\theta_{i+1}}(\varepsilon) \leftarrow f_{\theta_i}(\varepsilon) + \mathbf{V}_{p,q_{\theta_i}}(f_{\theta_i}(\varepsilon))$, which is implemented via the stop-gradient objective (1). In the limit, the training reaches a fixed point where the field \mathbf{V} vanishes. Under certain regularity assumptions one then obtains $p = q$.

Kernel Functions Throughout this paper, we use the term *kernel* to denote a symmetric bivariate function $k : \mathbb{R}^D \times \mathbb{R}^D \rightarrow \mathbb{R}$ that measures similarity between two points. Our analysis does not depend on positive definiteness or any other Mercer-type condition.

Definition 1 (Radial kernel). A kernel is called *radial* if it depends only on the squared distance: $k(\mathbf{x}, \mathbf{y}) = \phi(\|\mathbf{x} - \mathbf{y}\|^2)$ for radial profile $\phi : \mathbb{R} \rightarrow \mathbb{R}$.

Definition 2 (Kernel Density Estimate). Given a distribution p and a kernel k , the *kernel density estimate* (KDE) of p is

$$p_{\text{KDE}}[k](\mathbf{x}) := \mathbb{E}_{\mathbf{y} \sim p}[k(\mathbf{x}, \mathbf{y})]. \quad (4)$$

Note that the normalization factors in the drift field (3) are exactly the KDEs: $Z_p(\mathbf{x}) = p_{\text{KDE}}(\mathbf{x})$ and $Z_q(\mathbf{x}) = q_{\text{KDE}}(\mathbf{x})$. This connection between the drift field and KDEs will be central to our analysis.

Conservatism

Definition 3 (Conservative vector field). A vector field $\mathbf{V} : \mathbb{R}^D \rightarrow \mathbb{R}^D$ is **conservative** if there exists a scalar field $\mathcal{L} : \mathbb{R}^D \rightarrow \mathbb{R}$ such that $\mathbf{V}(\mathbf{x}) = -\nabla_{\mathbf{x}}\mathcal{L}(\mathbf{x})$ for all $\mathbf{x} \in \mathbb{R}^D$.

A standard characterization is that

Lemma 4. A vector field $V : \mathbb{R}^D \rightarrow \mathbb{R}^D$ is conservative if and only if its Jacobian is symmetric, i.e.

$$\frac{\partial \mathbf{V}_j}{\partial x_i} = \frac{\partial \mathbf{V}_i}{\partial x_j} \quad \text{for all } 1 \leq i, j \leq D.$$

Proof. See Section A. □

The difference of off-diagonals of the Jacobian measures the deviation from conservatism, which can be summarized in a generalized D -dimensional *curl*:

Definition 5 (Curl). The **curl** of a vector field $\mathbf{V} : \mathbb{R}^D \rightarrow \mathbb{R}^D$ is a h -dimensional vector

$$[\nabla \times \mathbf{V}]_{\frac{i(i-1)}{2} + j - 1} := \frac{\partial \mathbf{V}_i}{\partial x_j} - \frac{\partial \mathbf{V}_j}{\partial x_i} \quad \text{for } 1 \leq i < j \leq D \quad (5)$$

where $h = \frac{D(D-1)}{2}$. In particular, for $D = 2$, we get the scalar valued curl $\frac{\partial \mathbf{V}_x}{\partial y} - \frac{\partial \mathbf{V}_y}{\partial x}$.

Note that non-zero curl does not require the integral curves of \mathbf{V} to form closed loops. Curl also arises from *shear*—when the magnitude of the field varies transversally. This is worth emphasizing because it departs from the common intuition that curl implies circular flow, and for drifting fields in particular, curl is not a product of the flow’s direction, but rather the spatial variation in its magnitude.

Scalar Potentials and Conservative Training The stop-gradient objective (1) can implement any vector field \mathbf{V} as the sample update direction, including non-conservative ones. When $\mathbf{V}_{p,q}$ happens to be conservative, i.e., $\mathbf{V}_{p,q}(\mathbf{x}) = -\nabla_{\mathbf{x}}\mathcal{L}_{p,q}(\mathbf{x})$ for some scalar potential $\mathcal{L}_{p,q} : \mathbb{R}^D \rightarrow \mathbb{R}$,

Table 1: Sharp and flat kernels for common radial kernels. Derivations are provided in Theorems 15 to 17.

	Gaussian	Laplacian	Rational quadratic
Kernel $k(\mathbf{x}, \mathbf{y})$	$\exp(-\ \mathbf{x}-\mathbf{y}\ ^2/2\sigma^2)$	$\exp(-\ \mathbf{x}-\mathbf{y}\ /\sigma)$	$(1 + \ \mathbf{x}-\mathbf{y}\ ^2/\sigma^2)^{-2}$
Flat $k^b(\mathbf{x}, \mathbf{y})$	$\sigma^{-2} k(\mathbf{x}, \mathbf{y})$	$k(\mathbf{x}, \mathbf{y})/(\sigma\ \mathbf{x}-\mathbf{y}\)$	$\frac{4}{\sigma^2} k(\mathbf{x}, \mathbf{y})^{3/2}$
Sharp $k^\#(\mathbf{x}, \mathbf{y})$	$\sigma^2 k(\mathbf{x}, \mathbf{y})$	$\sigma(\ \mathbf{x}-\mathbf{y}\ + \sigma) k(\mathbf{x}, \mathbf{y})$	$\frac{\sigma^2}{2} k(\mathbf{x}, \mathbf{y})^{1/2}$

training simplifies:

$$\begin{aligned}
& \nabla_\theta \mathbb{E}_\varepsilon [\mathcal{L}^{\text{drift}}(\theta)] \\
&= \mathbb{E}_{\varepsilon \sim p_\varepsilon} [\nabla_\theta \|f_\theta(\varepsilon) - \text{sg}(f_\theta(\varepsilon) + \mathbf{V}_{p,q_\theta}(f_\theta(\varepsilon)))\|^2] \\
&= \mathbb{E}_{\varepsilon \sim p_\varepsilon} \left[\frac{\partial f_\theta(\varepsilon)}{\partial \theta}^\top \mathbf{V}_{p,q_\theta}(f_\theta(\varepsilon)) \right] \\
&= - \mathbb{E}_{\varepsilon \sim p_\varepsilon} \left[\frac{\partial f_\theta(\varepsilon)}{\partial \theta}^\top \nabla_x \mathcal{L}_{p,q_\theta}(f_\theta(\varepsilon)) \right] \\
&= - \nabla_\theta \mathbb{E}_{\mathbf{x} \sim q_\theta} [\mathcal{L}_{p,\text{sg}(q_\theta)}(\mathbf{x})].
\end{aligned} \tag{6}$$

That means training reduces to performing a gradient descent step with the scalar field $\mathbb{E}_{\mathbf{x} \sim q_\theta} [\mathcal{L}_{p,\text{sg}(q_\theta)}(\mathbf{x})]$ at each step, without explicitly constructing the transport field \mathbf{V} .

Note that the potential \mathcal{L} depends on the current generated distribution q_θ through the stop grad operation sg . This means the loss landscape inducing the sample movement shifts between training steps as q_θ evolves, and we are not descending a single fixed objective landscape, but a smoothly changing sequence of landscapes. Note that this is inherently different from, for example, the MMD loss where a truly fixed potential exists in which parameter values descent.

While the dependence on $\text{sg}(q_\theta)$ limits the direct applicability of standard optimization guarantees, the conservative formulation moves away from the V -centric framework of Deng et al. [2026], replacing the explicit construction and application of a transport field with a single scalar loss that can be implemented and optimized straightforwardly with standard automatic differentiation.

3 Drift Fields Are Not Generally Conservative

Plotting the rotation of the drift field sub field \mathbf{V}_p^+ or equivalently \mathbf{V}_q^- for different kernel choices reveals that, in general, the drift field is *not* conservative (see Figure 5).² While the Gaussian kernel yields a rotation of exactly zero, the Laplacian kernel and the rational quadratic kernel both produce nonzero rotations. This means no scalar potential \mathcal{L} exists whose gradient recovers these drift fields.³

The source of the non-conservatism is the position-dependent normalization by $Z(x)$. To see this, note that the unnormalized drifting fields $\mathbb{E}_p[k(\mathbf{x}, \mathbf{y})(\mathbf{y} - \mathbf{x})]$ coincides with the gradient of the scalar MMD objective for a particular kernel choice. We analyze this in the following section:

3.0.1 Nonconservatism is Caused by the Normalization

Deng et al. [2026] observe in Appendix C.2 that the drift field is closely related to the gradient of the squared MMD loss [Gretton et al., 2006], and, for the Gaussian kernel, derive a proportionality between the two. We reiterate this relation to show that the unnormalized field *is* conservative, and only through the introduction of the normalization, we get nonzero curl. Adopting our notation and

²We refer the reader to Section A.2 for a detailed discussion of why the conservatism of the sub fields is required.

³While we only provide a counterexample in 2D, counterexamples for arbitrary dimensions $D \geq 2$ follow by induction; see Section A.3.

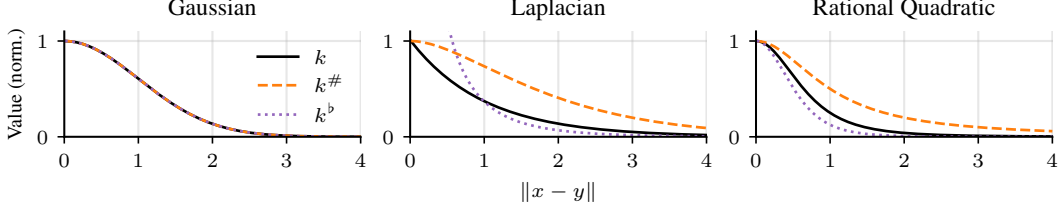


Figure 2: Sharp and flat kernel functions as a function of distance $\|x - y\|$ for the three kernels in Table 1. For the Gaussian kernel, k , $k^\#$, and k^b differ only by a constant factor. For the Laplacian and rational quadratic kernels, the sharp and flat kernels have qualitatively different shapes.

after some transformations (see Section C) the squared MMD loss is

$$\mathcal{L}^{\text{MMD}^2}[k](\theta) = \mathbb{E}_{\mathbf{x} \sim q_\theta} \left[\mathcal{L}_{p, \text{sg}(q_\theta)}^{\text{MMD}}[k](\mathbf{x}) \right], \quad (7)$$

where $\mathcal{L}_{p, \text{sg}(q_\theta)}^{\text{MMD}}[k](\mathbf{x}) = \mathbb{E}_{\mathbf{y}^- \sim \text{sg}(q_\theta)}[k(\mathbf{x}, \mathbf{y}^-)] - \mathbb{E}_{\mathbf{y}^+ \sim p}[k(\mathbf{x}, \mathbf{y}^+)]$.

For a radial kernel $k(\mathbf{x}, \mathbf{y}) = \phi(\|\mathbf{x} - \mathbf{y}\|^2)$, we identify the drift field $\mathbf{V}_{p,q}^{\text{MMD}}[k](\mathbf{x})$ of this objective as

$$\begin{aligned} \mathbf{V}_{p,q}^{\text{MMD}}[k](\mathbf{x}) &:= -\nabla_{\mathbf{x}} \mathcal{L}_{p, \text{sg}(q_\theta)}^{\text{MMD}}[k](\mathbf{x}) \\ &= \mathbb{E}_{\mathbf{y}^+ \sim p}[2\phi'(\|\mathbf{x} - \mathbf{y}^+\|^2)(\mathbf{y}^+ - \mathbf{x})] - \mathbb{E}_{\mathbf{y}^- \sim q}[2\phi'(\|\mathbf{x} - \mathbf{y}^-\|^2)(\mathbf{y}^- - \mathbf{x})]. \end{aligned} \quad (8)$$

For the Gaussian kernel, where $\phi' = -\frac{1}{2\sigma^2}\phi$, this is proportional to the unnormalized drifting field:

$$\mathbf{V}_{p,q}^{\text{unnorm.}}[k](\mathbf{x}) := \underbrace{\mathbb{E}_{\mathbf{y}^+ \sim p}[k(\mathbf{x}, \mathbf{y}^+)(\mathbf{y}^+ - \mathbf{x})]}_{:= \mathbf{V}_p^{\text{unnorm.}}} - \underbrace{\mathbb{E}_{\mathbf{y}^- \sim q}[k(\mathbf{x}, \mathbf{y}^-)(\mathbf{y}^- - \mathbf{x})]}_{:= \mathbf{V}_q^{\text{unnorm.}}}. \quad (9)$$

More generally if $\phi'(\|\mathbf{x} - \mathbf{y}\|^2)$ happens to align with another kernel, then we get its unnormalized drift field. The need to relate kernels losses like the MMD and those emerging in the corresponding drifting fields, motivates the following definition:

Flat and Sharp Kernels

Definition 6 (Sharp and flat). The **sharp** of a kernel k is the kernel $k^\#$ satisfying

$$\nabla_{\mathbf{x}} k^\#(\mathbf{x}, \mathbf{y}) = k(\mathbf{x}, \mathbf{y})(\mathbf{y} - \mathbf{x}). \quad (10)$$

The **flat** of k is the kernel k^b satisfying

$$\nabla_{\mathbf{x}} k(\mathbf{x}, \mathbf{y}) = k^b(\mathbf{x}, \mathbf{y})(\mathbf{y} - \mathbf{x}). \quad (11)$$

The notation is borrowed from musical accidentals: the sharp $k^\#$ raises the kernel (antiderivative), while the flat k^b lowers it (derivative). Note that by substituting Equation (10) into Equation (11) and vice-versa, it follows directly that $(k^\#)^b = (k^b)^\# = k$. Neither operation is guaranteed to exist in general, and neither preserves positive definiteness. The flat k^b requires k to be differentiable and may be singular where $\|\mathbf{x} - \mathbf{y}\| = 0$ (e.g., for the Laplacian kernel).

For a radial kernel $k(x, y) = \phi(\|\mathbf{x} - \mathbf{y}\|^2)$, both admit closed forms:

$$k^\#(\mathbf{x}, \mathbf{y}) = \frac{1}{2} \int_{\|\mathbf{x} - \mathbf{y}\|^2}^{\infty} \phi(r) dr, \quad k^b(\mathbf{x}, \mathbf{y}) = -2\phi'(\|\mathbf{x} - \mathbf{y}\|^2). \quad (12)$$

The flat-sharp formalism simplifies the discussion of the relation of MMD gradients and drifting fields:

Proposition 7. Let $k(\mathbf{x}, \mathbf{y})$ be a kernel for which $k^\#(\mathbf{x}, \mathbf{y})$ exists, then

$$\mathbf{V}_{p,q}^{\text{unnorm.}}[k](\mathbf{x}) = -\nabla_{\mathbf{x}} \mathcal{L}_{p, \text{sg}(q_\theta)}^{\text{MMD}}[k^\#](\mathbf{x}), \quad (13)$$

Proof.

$$\begin{aligned}
-\nabla_{\mathbf{x}} \mathcal{L}_{p, \text{sg}(q_\theta)}^{\text{MMD}}[k^\#](\mathbf{x}) &= \mathbb{E}_{\mathbf{y}^+ \sim p}[\nabla_{\mathbf{x}} k^\#(\mathbf{x}, \mathbf{y}^+)] - \mathbb{E}_{\mathbf{y}^- \sim \text{sg}(q_\theta)}[\nabla_{\mathbf{x}} k^\#(\mathbf{x}, \mathbf{y}^-)] \\
&= \mathbb{E}_{\mathbf{y}^+ \sim p}[k(\mathbf{x}, \mathbf{y}^+)(\mathbf{y}^+ - \mathbf{x})] - \mathbb{E}_{\mathbf{y}^- \sim q}[k(\mathbf{x}, \mathbf{y}^-)(\mathbf{y}^- - \mathbf{x})] \quad (14) \\
&= \mathbf{V}_{p,q}^{\text{unnorm.}}[k](\mathbf{x}).
\end{aligned}$$

□

It is thus conservative and has zero curl. The direction of the normalized field thus does *not* contribute to the non-conservatism. The normalization, which only changes the scale of the field, introduces a transversal variation in the fields magnitude which constitutes a *shear*. This shear is responsible for the non-zero curl (See discussion in Section 2).

Radiality is Necessary We have shown that if k is assumed to be radial then we find a potential given by the squared MMD whose gradient produces the unnormalized drifting field, which is thus, by definition, conservative. The reverse is also true. We refer the reader to Theorem 14 for the proof.

3.1 The Gaussian Kernel: An Exception where Normalization Retains Conservatism

The exception where the normalization does not lead to non-conservatism is the Gaussian kernel (see Figure 5, left). We are thus able to identify the exact scalar potential whose gradient produces the field:

Proposition 8. *For the Gaussian kernel with bandwidth σ , the drift sub-fields satisfy*

$$\mathbf{V}_p^+(\mathbf{x}) = \sigma^2 \nabla_{\mathbf{x}} \log p_{\text{KDE}}[k](\mathbf{x}), \quad \mathbf{V}_q^-(\mathbf{x}) = \sigma^2 \nabla_{\mathbf{x}} \log q_{\text{KDE}}[k](\mathbf{x}). \quad (15)$$

Proof. We compute $\nabla_{\mathbf{x}} \log q_{\text{KDE}}[k](\mathbf{x}) = \frac{\nabla_{\mathbf{x}} q_{\text{KDE}}[k](\mathbf{x})}{q_{\text{KDE}}[k](\mathbf{x})}$. Using Definition 2 and that we have for Gaussian kernel, that $\nabla_{\mathbf{x}} k(\mathbf{x}, \mathbf{y}) = \sigma^{-2} k(\mathbf{x}, \mathbf{y})(\mathbf{y} - \mathbf{x})$ (See Corollary 15 and Definition 6), we obtain:

$$\nabla_{\mathbf{x}} \log q_{\text{KDE}}[k](\mathbf{x}) = \frac{\mathbb{E}_q[\nabla_{\mathbf{x}} k(\mathbf{x}, \mathbf{y})]}{\mathbb{E}_q[k(\mathbf{x}, \mathbf{y})]} = \frac{1}{\sigma^2} \frac{\mathbb{E}_q[k(\mathbf{x}, \mathbf{y})(\mathbf{y} - \mathbf{x})]}{Z_q(\mathbf{x})} = \frac{1}{\sigma^2} \mathbf{V}_q^-(\mathbf{x}).$$

The same argument applies analogously to $\mathbf{V}_p^+(\mathbf{x})$. □

The composite drift field defined in Equation (3) thus reduces to

$$\mathbf{V}_{p,q}(\mathbf{x}) = \sigma^2 (\nabla_{\mathbf{x}} \log p_{\text{KDE}}[k](\mathbf{x}) - \nabla_{\mathbf{x}} \log q_{\text{KDE}}[k](\mathbf{x})) = -\sigma^2 \nabla_{\mathbf{x}} \log \left(\frac{q_{\text{KDE}}[k](\mathbf{x})}{p_{\text{KDE}}[k](\mathbf{x})} \right). \quad (16)$$

4 Sharp Normalization

Having found the normalization of the drifting field to be the culprit for nonconservatism, and that, in some cases, normalization does *not* destroy conservatism we propose a new normalization which restores conservatism for *any* radial kernel.

This normalization is given by

$$Z_p^\#(\mathbf{x}) := \mathbb{E}_{\mathbf{y}^+ \sim p}[k^\#(\mathbf{x}, \mathbf{y}^+)], \quad Z_q^\#(\mathbf{x}) := \mathbb{E}_{\mathbf{y}^- \sim q}[k^\#(\mathbf{x}, \mathbf{y}^-)] \quad (17)$$

for the positive and negative fields. Note that $Z_p^\# = p_{\text{KDE}}[k^\#]$ and $Z_q^\# = q_{\text{KDE}}[k^\#]$. By the defining property of the sharp kernel, $\nabla_{\mathbf{x}} k^\#(x, y) = k(x, y)(y - x)$, the gradient of the log sharp KDE recovers the drift numerator:

$$\begin{aligned}
\mathbf{V}_p^{\# +}(\mathbf{x}) &:= \frac{1}{Z_p^\#(\mathbf{x})} \mathbb{E}_{\mathbf{y}^+ \sim p}[k(\mathbf{x}, \mathbf{y}^+)(\mathbf{y}^+ - \mathbf{x})] = \nabla_{\mathbf{x}} \log p_{\text{KDE}}[k^\#](\mathbf{x}), \\
\mathbf{V}_q^{\# -}(\mathbf{x}) &:= \frac{1}{Z_q^\#(\mathbf{x})} \mathbb{E}_{\mathbf{y}^- \sim q}[k(\mathbf{x}, \mathbf{y}^-)(\mathbf{y}^- - \mathbf{x})] = \nabla_{\mathbf{x}} \log q_{\text{KDE}}[k^\#](\mathbf{x}).
\end{aligned} \quad (18)$$

Algorithm 1 Gaussian log-KDE Loss Pseudocode

```

def log_KDE_loss(x: "[N, D]", y_pos: "[N_pos, D]", y_neg: "[N_neg, D]", T: float):
    # compute pairwise distances
    dist_pos = cdist(x, y_pos)
    dist_neg = cdist(x, y_neg.detach())

    # compute logits (Gaussian)
    logits_pos = -dist_pos**2 / (2 * T**2)
    logits_neg = -dist_neg**2 / (2 * T**2)
    logits_neg.fill_diagonal_(-inf) # exclude diagonal

    # compute log KDE
    log_p = logsumexp(logits_pos, dim=1) - log(N_pos)
    log_q = logsumexp(logits_neg, dim=1) - log(N_neg - 1)

    # compute loss
    loss = (log_q - log_p).mean()
  
```

Definition 9 (Sharp-normalized drift field). We define the sharp-normalized drift field as

$$\mathbf{V}_{p,q}^\#(\mathbf{x}) := \mathbf{V}_p^{\#+}(\mathbf{x}) - \mathbf{V}_q^{\#-}(\mathbf{x}) = -\nabla_{\mathbf{x}} \log \left(\frac{q_{\text{KDE}}[k^\#](\mathbf{x})}{p_{\text{KDE}}[k^\#](\mathbf{x})} \right) \quad (19)$$

As $\mathbf{V}_{p,q}^\#(\mathbf{x})$ is conservative, we can use Equation (6) to obtain a well-defined, scalar training objective, the log-KDE loss:

$$\mathcal{L}_{p,q}^{\text{log-KDE}}(\theta) := \mathbb{E}_{\mathbf{x} \sim q_\theta} \left[\log \left(\frac{q_{\text{KDE}}[k^\#](\mathbf{x})}{p_{\text{KDE}}[k^\#](\mathbf{x})} \right) \right]. \quad (20)$$

Importantly, $q_{\text{KDE}}[k^\#](\mathbf{x}) = \mathbb{E}_{\mathbf{y}^- \sim \text{sg}(q_\theta)} [k^\#(\mathbf{y}^-, \mathbf{x})]$ is expected to only depend on θ through \mathbf{x} and not via \mathbf{y}^- here. As shown in Algorithm 1, for exponential kernels, the above objective can be implemented in a numerical-stable way using the `logsumexp` operation.

When Does Sharp-Normalized Field Coincide with the Drift Field? The sharp-normalized field and the drift field coincide (up to a global constant) if and only if $p_{\text{KDE}}[k^\#](\mathbf{x})/p_{\text{KDE}}[k](\mathbf{x})$ is independent of \mathbf{x} , which holds when $k^\# \propto k$. For radial kernels $k = \phi(\|\mathbf{x} - \mathbf{y}\|^2)$, this condition means:

$$\frac{1}{2} \int_{\|\mathbf{x}-\mathbf{y}\|^2}^{\infty} \phi(r) dr \propto \phi(\|\mathbf{x} - \mathbf{y}\|^2), \quad (21)$$

whose unique solution (up to scaling) is $\phi(r) = \exp(-r/2\sigma^2)$: the Gaussian kernel.

Proposition 10. *Among radial kernels, the Gaussian is the unique kernel for which the drift field and the sharp-normalized field coincide. It is characterized by the property $k^\# \propto k$.*

4.1 Comparing the Original and Sharp-Normalized Fields

Having established that sharp normalization restores conservatism, we now characterize how it differs from the original drift field and relate both to MMD-based training.

The vanilla $\mathbf{V}_{p,q}[k]$, MMD-induced $\mathbf{V}_{p,q}^{\text{MMD}}[k^\#]$ and log-KDE induced drift field $\mathbf{V}_{p,q}^\#$ all agree in the direction inducing terms $\mathbb{E}_{\mathbf{y}^+ \sim p}[k(\mathbf{x}, \mathbf{y}^+)(\mathbf{y}^+ - \mathbf{x})]$ and $\mathbb{E}_{\mathbf{y}^- \sim p}[k(\mathbf{x}, \mathbf{y}^-)(\mathbf{y}^- - \mathbf{x})]$, with field magnitudes differing due to the different normalizations. The difference in magnitude is most pronounced far away from the data. We illustrated the field magnitudes in 1D for three different kernel choices in Figure 3.

Interpretation. The visualization reveals that the three fields essentially implement three different levels of normalization:

- **No normalization:** the unnormalized drift field $\mathbf{V}_{p,q}^{\text{unnorm.}}[k]$ is the gradient of the MMD loss $\mathcal{L}_{p,\text{sg}(q_\theta)}^{\text{MMD}}[k^\#](\mathbf{x})$ and thus conservative but vanishes far away from data.

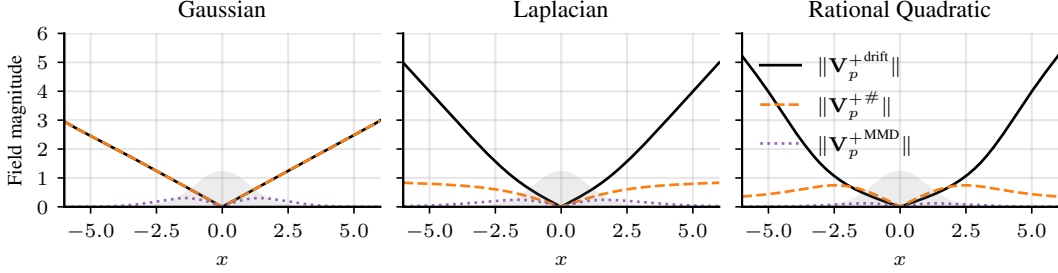


Figure 3: Given a fixed target distribution $p = \mathcal{N}(0, 1)$, we plot the field magnitudes of positive drift fields for different values of x . The gray shading shows the data density. The unnormalized MMD gradient decays in the tails. The drift field grows unboundedly. The sharp-normalized field lies between these extremes: it saturates for the Laplacian and decays slowly for the rational quadratic. For the Gaussian kernel, the drift field and the sharp-normalized field coincide. All three fields agree near the data.

- **Normalization by Z_p, Z_q :** The drift field $\mathbf{V}_{p,q}[k]$ of Deng et al. [2026] fixes the vanishing-signal problem but is, in general, not the gradient of a scalar loss.
- **Sharp normalization by $Z_p^\#, Z_q^\#$:** the sharp-normalized field $\mathbf{V}_{p,q}^\#$ is the gradient of the log-KDE loss (20) and thus conservative. Compared to the normalized MMD gradient, it shows improved tail behavior (e.g., bounded signal for the Laplacian kernel).

5 Experiments

We empirically compare the original drifting field objective against our proposed log-KDE loss to assess whether the non-conservative component of the drift field contributes to generation quality.

5.1 Experimental Setup

We train transformer-based models [Peebles and Xie, 2023] for class-conditional image generation on MNIST [LeCun et al., 2002] and Fashion-MNIST [Xiao et al., 2017]. To ensure a fair comparison, we fix all hyperparameters across experiments and vary only the training objective. Specifically, following Deng et al. [2026], we train a DiT-S/2 model with register tokens and style-embedding tokens using AdamW [Loshchilov and Hutter, 2017]. We train for 12,000 steps on MNIST and 16,000 steps on the more challenging Fashion-MNIST. Full configuration details are provided in Table 3.

Our primary goal is not to maximize absolute performance but rather to isolate and compare the effect of different training objectives on generation quality. We therefore deliberately omit several enhancements introduced by Deng et al. that are, in principle, applicable to any similarly structured objective. Concretely, we perform generation and loss computation in pixel space, do not employ any pretrained feature extractor, and do sample additional negative samples from the unconditional data distribution (CFG). Moreover, we use a single kernel width and a single loss term, and consequently omit the drifting-field normalization since there is no need to balance multiple objectives.

Kernel width normalization. To select kernel widths independently of the scale and structure of the data, we adopt a normalization strategy that differs slightly from that of Deng et al.. Inspired by Kynkäänniemi et al. [2019], we maintain, for each class, an exponential moving average ($\alpha=0.99$) of the mean ℓ_2 -distance from each data sample to its k -nearest neighbors ($k=5$) within a batch. Both real and generated samples are divided by this scalar before being passed to the loss function. To ensure proper initialization of the moving average, no optimization steps are taken during the first 300 batches.⁴ Kernel widths reported here are therefore not directly comparable to those in Deng et al. [2026].

⁴The learning rate schedule accounts for this additional warm-up period.

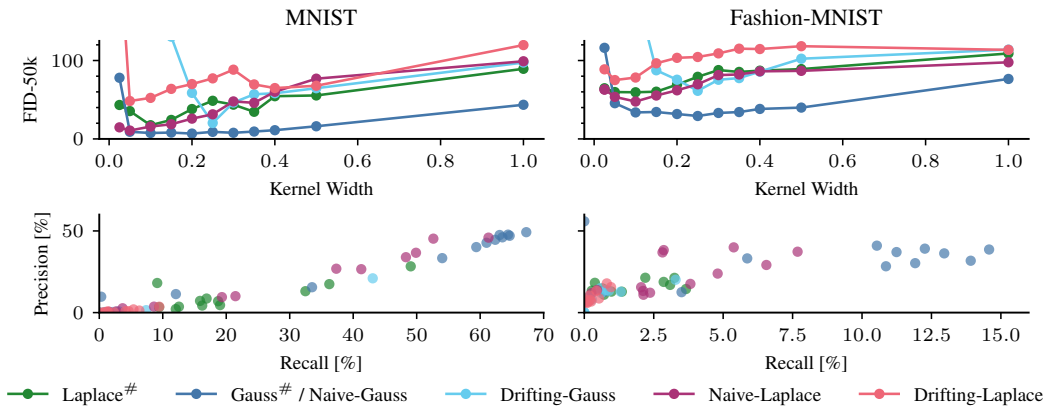


Figure 4: **Top:** Fréchet Inception Distance (FID-50k, lower is better) as a function of kernel width for MNIST (left) and Fashion-MNIST (right). **Bottom:** Corresponding precision and recall (higher is better) for all tested objectives and kernel widths.

Training objectives. The algorithm provided by Deng et al. does not compute the original drifting field as stated in Equation (3), even when the additional normalization over the batch dimension is omitted. Instead, when the numbers of positive and negative samples are equal, it computes

$$\bar{V}_{p,q}(x) = \frac{1}{(Z_p(\mathbf{x}) + Z_q(\mathbf{x}))^2} \mathbb{E}_{p,q} [k(\mathbf{x}, \mathbf{y}^+)k(\mathbf{x}, \mathbf{y}^-)(\mathbf{y}^+ - \mathbf{y}^-)], \quad (22)$$

which involves a different normalization term; a formal proof is given in Corollary 18. We therefore compare two variants in our experiments: the original algorithm of Deng et al. (including the additional batch-dimension normalization), and a variant that implements the objective exactly as stated in Equation (3) (see Algorithm 2 for an implementation). We refer to these as *Drifting-Laplace* and *Naive-Laplace*, respectively, where the *-Laplace* suffix indicates the choice of kernel function. We use *Gauss#* and *Laplace#* to refer to the log-KDE objective (Algorithm 1) with a Gaussian and Laplacian kernel respectively. Notice that *Gauss#* is mathematically equivalent to *Naive-Gauss* and we therefore report them together.

5.2 Results

Figure 4 reports the Fréchet Inception Distance [Heusel et al., 2017] computed over 50,000 samples (FID-50k), together with precision and recall [Kynkäänniemi et al., 2019], for each training objective as a function of kernel width. Table 2 summarizes these results by reporting the FID and corresponding $F1 = 2/(\text{Precision}^{-1} + \text{Recall}^{-1})$ for the best kernel width per objective. Uncurated generated samples are provided in Section E. All metrics are computed using the evaluation suite of ADM [Dhariwal and Nichol, 2021].

Naive drifting fields outperform the original algorithm. Models trained with the naive implementation of the drifting field consistently outperform those trained with the original algorithm on both datasets. On MNIST, Naive-Gauss achieves a FID of 6.81, compared to 20.38 for the corresponding objective of Deng et al.. Similar gaps are observed for the Laplacian kernel and on Fashion-MNIST. The naive Gaussian variant also exhibits greater robustness to the choice of kernel width than its original-algorithm counterpart.

Gaussian kernels outperform Laplacian kernels. Regardless of which implementation is used, Gaussian kernels consistently yield lower FID scores. On Fashion-MNIST, Naive-Gauss attains a FID of 29.25, whereas Naive-Laplace reaches only 47.68. The same trend holds on MNIST, suggesting that the Gaussian kernel provides a more effective training signal in these settings.

Sharp-normalized kernels are competitive with drifting fields. Laplace# achieves performance comparable to, though slightly worse than, Naive-Laplace across all tested kernel widths and both

Table 2: Best FID-50k (\downarrow) and corresponding F1 (\uparrow) for each objective.

Objective	MNIST			Fashion-MNIST		
	FID-50k \downarrow	F1 \uparrow	Best σ	FID-50k \downarrow	F1 \uparrow	Best σ
Gauss						
Gauss [#] / Naive-Gauss	6.81	0.57	0.20	29.25	0.21	0.25
Drifting-Gauss	20.38	0.28	0.25	61.37	0.06	0.25
Laplace						
Laplace [#]	17.48	0.36	0.10	59.50	0.05	0.10
Naive-Laplace	10.68	0.52	0.05	47.68	0.13	0.10
Drifting-Laplace	48.34	0.02	0.05	75.06	0.02	0.05

datasets (see Figure 4), indicating that the sharp normalization scheme yields an objective competitive with the drifting-field paradigm. Notably, Laplace[#] still substantially outperforms the original drifting implementation of Deng et al.

6 Conclusion

We have shown that drift fields are not generally conservative: the position-dependent normalization used by Deng et al. [2026] produces transversal magnitude variations for all radial kernels except the Gaussian. Using the sharp kernel $k^\#$, we introduced a sharp normalization that restores conservatism, yielding the log-KDE loss, a well-defined scalar objective. Our experiments confirm that sharp normalization performs comparably to the original drifting objective, suggesting that the non-conservative component is not required for high-quality generation.

Future work. On the practical side, we plan to validate the log-KDE loss at scale on ImageNet using the architecture and encoder of Deng et al. [2026]. On the theoretical side, a natural generalization is to replace log with a nonlinear link function g , yielding the potential $g(p_{\text{KDE}}[k^\#](\mathbf{x}))$ —conservative by construction for any differentiable g . The choice of g directly controls the tail behavior: $g = \text{id}$ recovers MMD (decaying tails), $g = \log$ gives the log-KDE loss (saturating tails for the Laplacian and increasing for the Gaussian kernel) and other choices such as the inverse of the radial profile ϕ^{-1} of a kernel, always produce linear growth when using this kernel as $k^\#$. We leave studying these configurations to future work.

References

- Mingyang Deng, He Li, Tianhong Li, Yilun Du, and Kaiming He. Generative modeling via drifting, 2026. URL <http://arxiv.org/abs/2602.04770>.
- Prafulla Dhariwal and Alexander Nichol. Diffusion models beat gans on image synthesis. *Advances in neural information processing systems*, 34:8780–8794, 2021.
- Arthur Gretton, Karsten Borgwardt, Malte Rasch, Bernhard Schölkopf, and Alex Smola. A kernel method for the two-sample-problem. *Advances in neural information processing systems*, 19, 2006.
- Martin Heusel, Hubert Ramsauer, Thomas Unterthiner, Bernhard Nessler, and Sepp Hochreiter. Gans trained by a two time-scale update rule converge to a local nash equilibrium. *Advances in neural information processing systems*, 30, 2017.
- Tuomas Kynkäänniemi, Tero Karras, Samuli Laine, Jaakko Lehtinen, and Timo Aila. Improved precision and recall metric for assessing generative models. *Advances in neural information processing systems*, 32, 2019.
- Yann LeCun, Léon Bottou, Yoshua Bengio, and Patrick Haffner. Gradient-based learning applied to document recognition. *Proceedings of the IEEE*, 86(11):2278–2324, 2002.
- Ilya Loshchilov and Frank Hutter. Decoupled weight decay regularization. *arXiv preprint arXiv:1711.05101*, 2017.

William Peebles and Saining Xie. Scalable diffusion models with transformers. In *Proceedings of the IEEE/CVF international conference on computer vision*, pages 4195–4205, 2023.

Han Xiao, Kashif Rasul, and Roland Vollgraf. Fashion-mnist: a novel image dataset for benchmarking machine learning algorithms. *arXiv preprint arXiv:1708.07747*, 2017.

A Conservatism and Jacobian Symmetry

We give a self-contained proof for Lemma 7, i.e.

A vector field $\mathbf{V} : \mathbb{R}^D \rightarrow \mathbb{R}^D$ is conservative if and only if its Jacobian is symmetric.

Proof. (\Rightarrow): If $\mathbf{V} = \nabla \mathcal{L}$, then $\frac{\partial \mathbf{V}_i}{\partial x_j} = \frac{\partial^2 \mathcal{L}}{\partial x_i \partial x_j} = \frac{\partial^2 \mathcal{L}}{\partial x_j \partial x_i} = \frac{\partial \mathbf{V}_j}{\partial x_i}$ by Schwarz's theorem.

(\Leftarrow): Assume the Jacobian of \mathbf{V} is symmetric. Define $\mathcal{L}(\mathbf{x}) := \int_0^1 \mathbf{V}(t\mathbf{x})^\top \mathbf{x} dt$. Then:

$$\begin{aligned} \frac{\partial \mathcal{L}}{\partial x_i} &= \int_0^1 \left(\mathbf{V}_i(t\mathbf{x}) + \sum_{j=1}^D \frac{\partial \mathbf{V}_j(t\mathbf{x})}{\partial x_i} x_j \right) dt \\ &= \int_0^1 \left(\mathbf{V}_i(t\mathbf{x}) + \sum_{j=1}^D t \frac{\partial \mathbf{V}_i(\mathbf{x})}{\partial x_j} \Big|_{\mathbf{x}=t\mathbf{x}} x_j \right) dt \\ &= \int_0^1 \left(\mathbf{V}_i(t\mathbf{x}) + t \frac{d}{dt} \mathbf{V}_i(t\mathbf{x}) \right) dt = \int_0^1 \frac{d}{dt} [t \mathbf{V}_i(t\mathbf{x})] dt = \mathbf{V}_i(\mathbf{x}), \end{aligned}$$

where the second line uses the chain rule $\frac{\partial \mathbf{V}_j(t\mathbf{x})}{\partial x_i} = t \frac{\partial \mathbf{V}_j(\mathbf{x})}{\partial x_i} \Big|_{\mathbf{x}=t\mathbf{x}}$ and the symmetry assumption $\frac{\partial \mathbf{V}_j}{\partial x_i} = \frac{\partial \mathbf{V}_i}{\partial x_j}$. Thus $\nabla \mathcal{L} = \mathbf{V}$. \square

A.1 Curl of Selected Drifting Fields

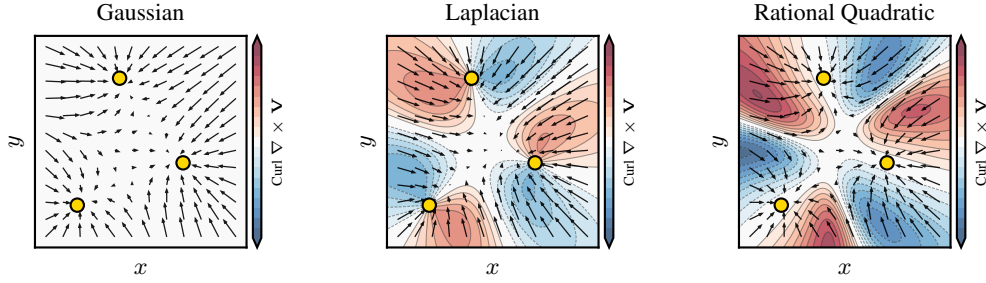


Figure 5: Scalar curl of the positive drifting field for three different kernels. *Left:* for the Gaussian kernel the drifting field has no rotation and *can* be expressed as the gradient of a scalar. *Center:* For the Laplacian kernel we see that the curl does *not* vanish and thus no potential exists which recovers the field. *Right:* Also for the rational quadratic kernel the rotation is non-zero. This illustrates that the Gaussian kernel is the exception when it comes to the fields conservatism.

A.2 Relation of conservatism of $\mathbf{V}_{p,q}$ and \mathbf{V}_p^+ and \mathbf{V}_q^-

Note that for showing nonconservatism, in general, of the composite field $\mathbf{V}_{p,q}$, it is sufficient to show that either of the sub fields \mathbf{V}_p^+ or \mathbf{V}_q^- are nonconservative. This is because both p and q can be varied independently. While it is true that the sum of two nonconservative fields can be, again, conservative in the case that curling components of the fields cancel out, we can realize that the conservatism of both fields is required, by fixing, for example, p and then moving \mathbf{V}_q^- to a region where $\mathbf{V}_p^+ \rightarrow 0$. If this region exists, then \mathbf{V}_p^+ cannot cancel the rotation of \mathbf{V}_q^- , and thus \mathbf{V}_q^- must have individually zero curl. For all analyzed kernels this region exists far away from the data p . The same argument applies when fixing \mathbf{V}_q^- .

A.3 Nonconservatism in Arbitrary Dimensions

We show that a single counterexample in \mathbb{R}^2 suffices to establish nonconservatism in all dimensions $D \geq 2$.

Lemma 11 (Restriction preserves conservatism). *Let $f : \mathbb{R}^{D+1} \rightarrow \mathbb{R}^{D+1}$ be conservative with potential \mathcal{L} , and fix $c \in \mathbb{R}$. Define $g : \mathbb{R}^D \rightarrow \mathbb{R}^D$ by $g_i(\mathbf{x}) = f_i(x_1, \dots, x_D, c)$ for $i = 1, \dots, D$. Then g is conservative with potential $\tilde{\mathcal{L}}(\mathbf{x}) = \mathcal{L}(x_1, \dots, x_D, c)$.*

Proof. Since $f = \nabla \mathcal{L}$, we have $g_i(\mathbf{x}) = \frac{\partial \mathcal{L}}{\partial x_i} \Big|_{x_{D+1}=c} = \frac{\partial}{\partial x_i} \mathcal{L}(\mathbf{x}, c) = \frac{\partial \tilde{\mathcal{L}}}{\partial x_i}(\mathbf{x})$, so $g = \nabla \tilde{\mathcal{L}}$. \square

Lemma 12 (Embedding of drift fields). *Let $\mathbf{y}_1, \dots, \mathbf{y}_M \in \mathbb{R}^D$ and define $\tilde{\mathbf{y}}_m = (\mathbf{y}_m, 0) \in \mathbb{R}^{D+1}$. Denote by \mathbf{V}_p^+ the drift sub-field in \mathbb{R}^D with data $\{\mathbf{y}_m\}$ and by $\widetilde{\mathbf{V}}_p^+$ the drift sub-field in \mathbb{R}^{D+1} with data $\{\tilde{\mathbf{y}}_m\}$. Then for all $\mathbf{x} \in \mathbb{R}^D$:*

$$\mathbf{V}_p^+(\mathbf{x}) = \left(\widetilde{\mathbf{V}}_p^+(\mathbf{x}, 0) \right)_{1:D},$$

where $(\cdot)_{1:D}$ denotes the first D components.

Proof. At $\tilde{\mathbf{x}} = (\mathbf{x}, 0)$, we have $\|\tilde{\mathbf{x}} - \tilde{\mathbf{y}}_m\|^2 = \|\mathbf{x} - \mathbf{y}_m\|^2$, so $k(\tilde{\mathbf{x}}, \tilde{\mathbf{y}}_m) = k(\mathbf{x}, \mathbf{y}_m)$. The first D components of the $(D+1)$ -dimensional field are

$$\left(\widetilde{\mathbf{V}}_p^+(\mathbf{x}, 0) \right)_{1:D} = \frac{\sum_m k(\mathbf{x}, \mathbf{y}_m)(\mathbf{y}_m - \mathbf{x})}{\sum_m k(\mathbf{x}, \mathbf{y}_m)} = \mathbf{V}_p^+(\mathbf{x}).$$

\square

Proposition 13. *If $\mathbf{y}_1, \dots, \mathbf{y}_M \in \mathbb{R}^D$ is a counterexample to conservatism, then $\tilde{\mathbf{y}}_1, \dots, \tilde{\mathbf{y}}_M \in \mathbb{R}^{D+1}$ is a counterexample in \mathbb{R}^{D+1} .*

Proof. By contrapositive. Suppose $\widetilde{\mathbf{V}}_p^+$ were conservative. By Theorem 11, restricting to $\{x_{D+1} = 0\}$ and taking the first D components yields a conservative field. By Theorem 12, this restricted field equals \mathbf{V}_p^+ , contradicting the assumption that $\{\mathbf{y}_m\}$ is a counterexample. \square

Since we exhibit a counterexample in $D = 2$ (see Figure 5), it follows by induction that counterexamples to conservatism of normalized drift fields exist in all dimensions $D \geq 2$.

A.4 Radiality is a Requirement for Conservatism

Lemma 14. *When the field $\mathbf{V}_{p,q}^{\text{unnorm.}}[k](\mathbf{x})$ is conservative k must be a **radial** kernel.*

Proof. For the field to be generally conservative both components must be conservative individually. We thus know that the inside of the expectation $u(\mathbf{x}, \mathbf{y}) := k(\mathbf{x}, \mathbf{y})(\mathbf{y} - \mathbf{x})$ has to have a symmetric Jacobian: $\frac{\partial}{\partial x_j} [k(\mathbf{x}, \mathbf{y})(\mathbf{y}_i - \mathbf{x}_i)] = \frac{\partial}{\partial x_i} [k(\mathbf{x}, \mathbf{y})(\mathbf{y}_j - \mathbf{x}_j)]$ for all $i \neq j$. Rearranging this we get:

$$\frac{\frac{\partial k}{\partial x_j}}{\frac{\partial k}{\partial x_i}} = \frac{\mathbf{y}_j - \mathbf{x}_j}{\mathbf{y}_i - \mathbf{x}_i},$$

This reads as: *the ratio of individual components equals between the difference $\mathbf{x} - \mathbf{y}$ and the gradient vector $\nabla_{\mathbf{x}} k(\mathbf{x}, \mathbf{y})$. This requires $\nabla_{\mathbf{x}} k(\mathbf{x}, \mathbf{y}) \parallel (\mathbf{y} - \mathbf{x})$. Setting $\mathbf{y} = 0$ without loss of generality, this means $\nabla_{\mathbf{x}} k(\mathbf{x}, 0) \parallel \mathbf{x}$. Since the gradient is everywhere radial, k must be constant on spheres centered at \mathbf{y} , hence $k(\mathbf{x}, \mathbf{y}) = \phi(\|\mathbf{x} - \mathbf{y}\|^2)$. \square*

B Detailed Kernel Derivations

This appendix provides detailed derivations for the sharp and flat kernels of common radial kernels, supporting the summary given in Table 1.

B.1 Gaussian Kernel

Corollary 15. For the Gaussian kernel, we have $k^\#(\mathbf{x}, \mathbf{y}) = \sigma^2 k(\mathbf{x}, \mathbf{y})$ and $k^b(\mathbf{x}, \mathbf{y}) = \frac{1}{\sigma^2} k(\mathbf{x}, \mathbf{y})$, so both are proportional to k .

Proof. Consider the Gaussian kernel with bandwidth σ :

$$k(\mathbf{x}, \mathbf{y}) = \exp\left(-\frac{\|\mathbf{x} - \mathbf{y}\|^2}{2\sigma^2}\right)$$

In radial form, this corresponds to $\phi(r) = \exp(-r/(2\sigma^2))$.

Computing the sharp: Using the general formula for radial kernels:

$$\begin{aligned} k^\#(\mathbf{x}, \mathbf{y}) &= \frac{1}{2} \int_{\|\mathbf{x}-\mathbf{y}\|^2}^{\infty} \phi(r) \, dr = \frac{1}{2} \int_{\|\mathbf{x}-\mathbf{y}\|^2}^{\infty} e^{-r/(2\sigma^2)} \, dr \\ &= \frac{1}{2} \left[-2\sigma^2 e^{-r/(2\sigma^2)} \right]_{\|\mathbf{x}-\mathbf{y}\|^2}^{\infty} = \sigma^2 k(\mathbf{x}, \mathbf{y}) \end{aligned}$$

Computing the flat: We have $\phi'(r) = -\frac{1}{2\sigma^2} e^{-r/(2\sigma^2)}$. Then:

$$k^b(\mathbf{x}, \mathbf{y}) = -2\phi'(\|\mathbf{x} - \mathbf{y}\|^2) = \frac{1}{\sigma^2} e^{-\|\mathbf{x}-\mathbf{y}\|^2/(2\sigma^2)} = \frac{1}{\sigma^2} k(\mathbf{x}, \mathbf{y})$$

Thus both the sharp and flat are proportional to the original Gaussian kernel. \square

B.2 Laplacian Kernel

Corollary 16. For the Laplacian kernel $k(\mathbf{x}, \mathbf{y}) = \exp(-\|\mathbf{x} - \mathbf{y}\|/\sigma)$, the sharp is $k^\#(\mathbf{x}, \mathbf{y}) = \sigma(\|\mathbf{x} - \mathbf{y}\| + \sigma)k(\mathbf{x}, \mathbf{y})$ and the flat is $k^b(\mathbf{x}, \mathbf{y}) = \frac{k(\mathbf{x}, \mathbf{y})}{\sigma\|\mathbf{x}-\mathbf{y}\|}$.

Proof. The Laplacian kernel is $k(\mathbf{x}, \mathbf{y}) = \exp(-\|\mathbf{x} - \mathbf{y}\|/\sigma)$. In radial form, $\phi(r) = \exp(-\sqrt{r}/\sigma)$ where $r = \|\mathbf{x} - \mathbf{y}\|^2$.

Computing the sharp: Using the general formula:

$$k^\#(\mathbf{x}, \mathbf{y}) = \frac{1}{2} \int_{\|\mathbf{x}-\mathbf{y}\|^2}^{\infty} \exp(-\sqrt{r}/\sigma) \, dr$$

Let $u = \sqrt{r}$, so $r = u^2$ and $dr = 2u \, du$. When $r = \|\mathbf{x} - \mathbf{y}\|^2$, we have $u = \|\mathbf{x} - \mathbf{y}\|$:

$$k^\#(\mathbf{x}, \mathbf{y}) = \int_{\|\mathbf{x}-\mathbf{y}\|}^{\infty} u \exp(-u/\sigma) \, du$$

Using integration by parts:

$$\begin{aligned} &= [-\sigma u \exp(-u/\sigma)]_{\|\mathbf{x}-\mathbf{y}\|}^{\infty} + \sigma \int_{\|\mathbf{x}-\mathbf{y}\|}^{\infty} \exp(-u/\sigma) \, du \\ &= \sigma \|\mathbf{x} - \mathbf{y}\| \exp(-\|\mathbf{x} - \mathbf{y}\|/\sigma) + \sigma^2 \exp(-\|\mathbf{x} - \mathbf{y}\|/\sigma) \\ &= \sigma(\|\mathbf{x} - \mathbf{y}\| + \sigma)k(\mathbf{x}, \mathbf{y}) \end{aligned}$$

Computing the flat: For $\phi(r) = \exp(-\sqrt{r}/\sigma)$, we have:

$$\phi'(r) = -\frac{1}{2\sigma\sqrt{r}} \exp(-\sqrt{r}/\sigma)$$

Therefore:

$$k^b(\mathbf{x}, \mathbf{y}) = -2\phi'(\|\mathbf{x} - \mathbf{y}\|^2) = \frac{1}{\sigma\|\mathbf{x} - \mathbf{y}\|} \exp(-\|\mathbf{x} - \mathbf{y}\|/\sigma) = \frac{k(\mathbf{x}, \mathbf{y})}{\sigma\|\mathbf{x} - \mathbf{y}\|}$$

\square

B.3 Rational Quadratic Kernel

Corollary 17. For the rational quadratic kernel $k(\mathbf{x}, \mathbf{y}) = (1 + \|\mathbf{x} - \mathbf{y}\|^2/\sigma^2)^{-2}$, the sharp is $k^\#(\mathbf{x}, \mathbf{y}) = \frac{\sigma^2}{2} k(\mathbf{x}, \mathbf{y})^{1/2}$ and the flat is $k^\flat(\mathbf{x}, \mathbf{y}) = \frac{4}{\sigma^2} k(\mathbf{x}, \mathbf{y})^{3/2}$.

Proof. In radial form, $\phi(r) = (1 + r/\sigma^2)^{-2}$.

Computing the sharp:

$$k^\#(\mathbf{x}, \mathbf{y}) = \frac{1}{2} \int_{\|\mathbf{x}-\mathbf{y}\|^2}^{\infty} (1 + r/\sigma^2)^{-2} dr$$

Let $t = 1 + r/\sigma^2$, so $dr = \sigma^2 dt$:

$$\begin{aligned} k^\#(\mathbf{x}, \mathbf{y}) &= \frac{\sigma^2}{2} \int_{1+\|\mathbf{x}-\mathbf{y}\|^2/\sigma^2}^{\infty} t^{-2} dt = \frac{\sigma^2}{2} [-t^{-1}]_{1+\|\mathbf{x}-\mathbf{y}\|^2/\sigma^2}^{\infty} \\ &= \frac{\sigma^2}{2} (1 + \|\mathbf{x} - \mathbf{y}\|^2/\sigma^2)^{-1} = \frac{\sigma^2}{2} k(\mathbf{x}, \mathbf{y})^{1/2} \end{aligned}$$

Computing the flat: We have $\phi'(r) = -\frac{2}{\sigma^2} (1 + r/\sigma^2)^{-3}$. Then:

$$k^\flat(\mathbf{x}, \mathbf{y}) = -2\phi'(\|\mathbf{x} - \mathbf{y}\|^2) = \frac{4}{\sigma^2} (1 + \|\mathbf{x} - \mathbf{y}\|^2/\sigma^2)^{-3} = \frac{4}{\sigma^2} k(\mathbf{x}, \mathbf{y})^{3/2}$$

□

C Squared MMD as a Stop-Gradient Objective

We show how the squared MMD loss can be cast into the stop-gradient form used in the main text. The squared MMD between two distributions p and q with kernel k is

$$\text{MMD}_k^2(p, q_\theta) = \mathbb{E}_{p,p}[k(\mathbf{y}, \mathbf{y}')] - 2\mathbb{E}_{p,q_\theta}[k(\mathbf{y}, \mathbf{x})] + \mathbb{E}_{q_\theta,q_\theta}[k(\mathbf{x}, \mathbf{x}')].$$

Calculating the gradient of the repulsion term $\mathbb{E}_{q_\theta,q_\theta}[k(\mathbf{x}, \mathbf{x}')] we get$

$$\nabla_\theta \mathbb{E}_{q_\theta,q_\theta}[k(\mathbf{x}, \mathbf{x}')] = \mathbb{E}_{\varepsilon,\varepsilon'} [\nabla_{\mathbf{x}} k(\mathbf{x}, \mathbf{x}')^\top \nabla_\theta f_\theta(\varepsilon) + \nabla_{\mathbf{x}'} k(\mathbf{x}, \mathbf{x}')^\top \nabla_\theta f_\theta(\varepsilon')].$$

By symmetry of k , i.e. $k(\mathbf{x}, \mathbf{x}') = k(\mathbf{x}', \mathbf{x})$, and by the identical distribution of ε and ε' , both terms have the same expectation. This thus can be expressed with the sg as:

$$2\nabla_\theta \mathbb{E}_{q_\theta, \text{sg}(q_\theta)}[k(\mathbf{x}, \mathbf{x}')]]$$

Dropping the p, p term and the scalar factor 2, we get the following by unifying the expectations over q_θ :

$$\begin{aligned} \mathcal{L}_k^{\text{MMD}^2}(\theta) &= \mathbb{E}_{\mathbf{x} \sim q_\theta} \left[\underbrace{\mathbb{E}_{\mathbf{y}^- \sim \text{sg}(q_\theta)}[k(\mathbf{x}, \mathbf{y}^-)] - \mathbb{E}_{\mathbf{y}^+ \sim p}[k(\mathbf{x}, \mathbf{y}^+)]}_{=: \mathcal{L}_{p, \text{sg}(q_\theta)}^{\text{MMD}}[k](\mathbf{x})} \right], \end{aligned}$$

which has a θ -gradient equals $\frac{1}{2} \nabla_\theta \text{MMD}_k^2(p, q_\theta)$. The inner function $\mathcal{L}_{p, \text{sg}(q_\theta)}^{\text{MMD}}[k](\mathbf{x})$ is the per-sample MMD potential whose $\nabla_{\mathbf{x}}$ gradient defines the MMD-induced field via Equation (6).

D Wrong Drifting Normalization

Corollary 18. The pseudocode given by [Deng et al. \[2026\]](#) in Algorithm 2, does not produce the original drifting field

$$\mathbf{V}_{p,q}(\mathbf{x}) = \frac{1}{Z_p(\mathbf{x})Z_q(\mathbf{x})} \mathbb{E}_{p,q} [k(\mathbf{x}, \mathbf{y}^+)k(\mathbf{x}, \mathbf{y}^-)(\mathbf{y}^+ - \mathbf{y}^-)] \quad (23)$$

, even if the additional normalization over the batch dimension is omitted. Here,

$$Z_p(\mathbf{x}) = \mathbb{E}_p [k(\mathbf{x}, \mathbf{y}^+)] \approx \frac{1}{N_{pos}} \sum_{j=1}^{N_{pos}} k(\mathbf{x}, \mathbf{y}_j^+) \quad (24)$$

$$Z_q(\mathbf{x}) = \mathbb{E}_q [k(\mathbf{x}, \mathbf{y}^-)] \approx \frac{1}{N_{neg}} \sum_{j=1}^{N_{neg}} k(\mathbf{x}, \mathbf{y}_j^-) \quad (25)$$

denote the drift normalization factors that are computed using the Monte Carlo method. Instead, for the common case $N_{pos} = N_{neg} = N$, the algorithm from Deng et al. [2026] produces the field

$$\bar{V}_{p,q}(x) = \frac{1}{(Z_p(\mathbf{x}) + Z_q(\mathbf{x}))^2} \mathbb{E}_{p,q} [k(\mathbf{x}, \mathbf{y}^+)k(\mathbf{x}, \mathbf{y}^-)(\mathbf{y}^+ - \mathbf{y}^-)]. \quad (26)$$

Proof. We proceed by analyzing the code line-by-line.

```
# x: [N, D]
# y_pos: [N_pos, D]
# y_neg: [N_neg, D]
# T: temperature

# compute pairwise distance
dist_pos = cdist(x, y_pos) # [N, N_pos]
dist_neg = cdist(x, y_neg) # [N, N_neg]

# ignore self (if y_neg is x)
dist_neg += eye(N) * 1e6

# compute logits
logit_pos = -dist_pos / T
logit_neg = -dist_neg / T

# concat for normalization
logit = cat([logit_pos, logit_neg], dim=1)
```

The first part calculates the logits of the exponential kernel $[\mathbf{l}]_{i,j} = \log k(\mathbf{x}_i, \mathbf{y}_j)$ between generated samples \mathbf{x}_i and positive and negative samples $\mathbf{y}_j^+, \mathbf{y}_j^-$, respectively. Here, we use \mathbf{y} (without plus or minus) to denote the concatenated target matrix $\mathbf{y} = (\mathbf{y}_1^+, \dots, \mathbf{y}_{N_{pos}}^+, \mathbf{y}_1^-, \dots, \mathbf{y}_{N_{neg}}^-)$.

```
# normalize (normalization over batch dim has been omitted!)
A_row = logit.softmax(dim=-1)
A = A_row
```

Next, the softmax operation is applied across the j -dimension to calculate the kernels and normalize simultaneously in a numerical stable fashion. Assuming that the Monte Carlo approximations in (24) and (25) hold exactly, i.e. that $Z_p(\mathbf{x}) = \frac{1}{N_{pos}} \sum_{n=1}^{N_{pos}} k(\mathbf{x}, \mathbf{y}_n^+)$ and $Z_q(\mathbf{x}) = \frac{1}{N_{neg}} \sum_{n=1}^{N_{neg}} k(\mathbf{x}, \mathbf{y}_n^-)$, we obtain

$$[\mathbf{A}]_{i,j} = \frac{\exp(\mathbf{l}_{i,j})}{\sum_{n=1}^{N_{pos}+N_{neg}} \exp(\mathbf{l}_{i,n})} = \frac{k(\mathbf{x}_i, \mathbf{y}_j)}{\sum_{n=1}^{N_{pos}} k(\mathbf{x}_i, \mathbf{y}_n^+) + \sum_{n=1}^{N_{neg}} k(\mathbf{x}_i, \mathbf{y}_n^-)} \quad (27)$$

$$= \frac{k(\mathbf{x}_i, \mathbf{y}_j)}{N_{pos}Z_p(\mathbf{x}_i) + N_{neg}Z_q(\mathbf{x}_i)}. \quad (28)$$

Notice that, due to the concatenation, the normalization factor is $N_{pos}Z_p(\mathbf{x}_i) + N_{neg}Z_q(\mathbf{x}_i)$. If, instead, the softmax were to be taken across \mathbf{y}^+ and \mathbf{y}^- independently, the softmax operation would correctly yield the normalization factors $N_{pos}Z_p(\mathbf{x}_i)$ and $N_{neg}Z_q(\mathbf{x}_i)$.

```
# back to [N, N_pos] and [N, N_neg]
A_pos, A_neg = A[:, :N_pos], A[:, N_pos:]

# compute the weights
W_pos = A_pos # [N, N_pos]
```

```

W_neg = A_neg # [N, N_neg]
W_pos *= A_neg.sum(dim=1, keepdim=True)
W_neg *= A_pos.sum(dim=1, keepdim=True)

```

Next, the weights for the individual \mathbf{y}_j^+ and \mathbf{y}_j^- are calculated. Assuming $N_{\text{pos}} = N_{\text{neg}} = N$ from here on yields

$$[\mathbf{W}_{\text{pos}}]_{i,j} = \frac{k(\mathbf{x}_i, \mathbf{y}_j^+)}{N(Z_p(\mathbf{x}_i) + Z_q(\mathbf{x}_i))} \sum_{n=1}^N \frac{k(\mathbf{x}_i, \mathbf{y}_n^-)}{N(Z_p(\mathbf{x}_i) + Z_q(\mathbf{x}_i))} \quad (29)$$

$$= \frac{Z_q(\mathbf{x}_i)k(\mathbf{x}_i, \mathbf{y}_j^+)}{N(Z_p(\mathbf{x}_i) + Z_q(\mathbf{x}_i))^2} \quad (30)$$

, for the positive weights. Likewise for \mathbf{W}_{neg} , we obtain

$$[\mathbf{W}_{\text{neg}}]_{i,j} = \frac{Z_p(\mathbf{x}_i)k(\mathbf{x}_i, \mathbf{y}_j^-)}{N(Z_p(\mathbf{x}_i) + Z_q(\mathbf{x}_i))^2}. \quad (31)$$

```

drift_pos = W_pos @ y_pos # [N, D]
drift_neg = W_neg @ y_neg # [N, D]

v = drift_pos - drift_neg
return v

```

The final step involves taking a weighted sum over \mathbf{y}^+ and \mathbf{y}^- and subtracting them from each other to obtain the drifting field $\bar{\mathbf{V}}_{p,q}$. Substituting (30) and (31) into this sum yields

$$\bar{\mathbf{V}}_{p,q}(\mathbf{x}_i) = \sum_{j=1}^N [\mathbf{W}_{\text{pos}}]_{i,j} \mathbf{y}_j^+ - \sum_{j=1}^N [\mathbf{W}_{\text{neg}}]_{i,j} \mathbf{y}_j^- \quad (32)$$

$$= \frac{Z_q(\mathbf{x}_i) \frac{1}{N} \sum_{j=1}^N k(\mathbf{x}_i, \mathbf{y}_j^+) \mathbf{y}_j^+ - Z_p(\mathbf{x}_i) \frac{1}{N} \sum_{j=1}^N k(\mathbf{x}_i, \mathbf{y}_j^-) \mathbf{y}_j^-}{(Z_p(\mathbf{x}_i) + Z_q(\mathbf{x}_i))^2} \quad (33)$$

Finally, we can substitute (24) and (25) into (33):

$$\bar{\mathbf{V}}_{p,q}(\mathbf{x}_i) = \frac{\mathbb{E}_q[k(\mathbf{x}_i, \mathbf{y}^-)] \mathbb{E}_p[k(\mathbf{x}_i, \mathbf{y}^+) \mathbf{y}^+] - \mathbb{E}_p[k(\mathbf{x}_i, \mathbf{y}^+)] \mathbb{E}_q[k(\mathbf{x}_i, \mathbf{y}^-) \mathbf{y}^-]}{(Z_p(\mathbf{x}_i) + Z_q(\mathbf{x}_i))^2}. \quad (34)$$

As $\mathbb{E}_q[k(\mathbf{x}_i, \mathbf{y}^-)]$ is constant w.r.t. \mathbf{y}^+ and $\mathbb{E}_p[k(\mathbf{x}_i, \mathbf{y}^+)]$ is constant w.r.t. \mathbf{y}^- and moreover $p \perp\!\!\!\perp q$, we can take the expectation over the joint distribution $(\mathbf{y}^+, \mathbf{y}^-) \sim p(\mathbf{y}^+)q(\mathbf{y}^-)$ to obtain

$$\bar{\mathbf{V}}_{p,q}(\mathbf{x}_i) = \frac{1}{(Z_p(\mathbf{x}_i) + Z_q(\mathbf{x}_i))^2} \mathbb{E}_{p,q} [k(\mathbf{x}_i, \mathbf{y}^+)k(\mathbf{x}_i, \mathbf{y}^-)(\mathbf{y}^+ - \mathbf{y}^-)]. \quad (35)$$

□

D.1 Naive Drifting Algorithm

Algorithm 2 implements the original drifting field as given by (3).

Algorithm 2 Compute Drifting Field Naively (i.e. as in Equation (3))

```

def compute_V(x: "[N, D]", y_pos: "[N_pos, D]", y_neg: "[N_neg, D]", T: float):
    # compute pairwise distance
    dist_pos = cdist(x, y_pos) # [N, N_pos]
    dist_neg = cdist(x, y_neg) # [N, N_neg]

    # compute logits
    logit_pos = -dist_pos / T
    logit_neg = -dist_neg / T
    logit_neg.fill_diagonal_(-inf)

    # compute normalized kernels
    # k(x, y+) / (N + Z_p) and k(x, y-) / (N + Z_n)
    A_pos = logit_pos.softmax(dim=-1) # [N, N_pos]
    A_neg = logit_neg.softmax(dim=-1) # [N, N_neg]

    # compute product
    # k(x, y+)k(x, y-) / (N^2 + Z_p * Z_q)
    A = A_pos[:, :, None] * A_neg[:, None, :] # [N, N_pos, N_neg]

    # compute weights
    # Z_q k(x, y+) / (N * Z_p * Z_q)
    # Z_p k(x, y-) / (N * Z_p * Z_q)
    W_pos = A.sum(dim=2) # [N, N_pos]
    W_neg = A.sum(dim=1) # [N, N_neg]

    # compute drift field V
    drift_pos = W_pos @ y_pos # [N, D]
    drift_neg = W_neg @ y_neg # [N, D]
    V = drift_pos - drift_neg
  
```

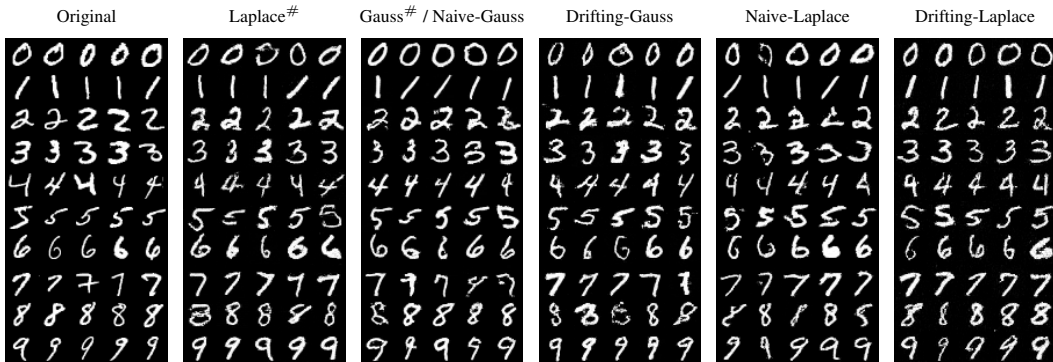
E Additional Results


Figure 6: Uncurated set of generated images on MNIST.

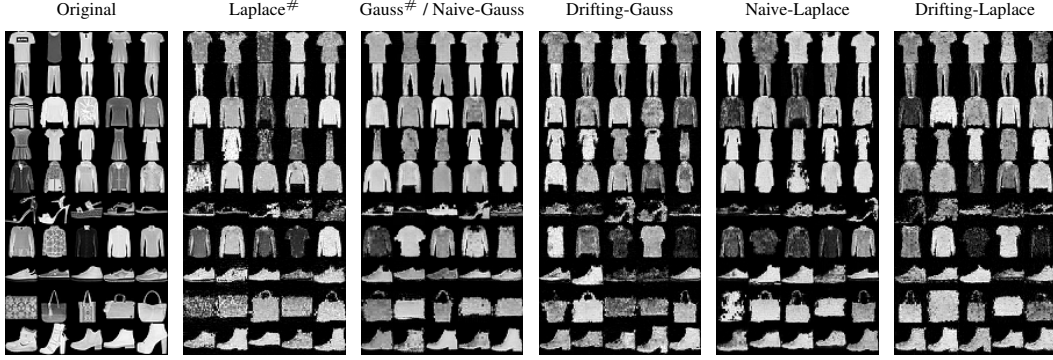


Figure 7: Uncurated set of generated images on Fashion-MNIST.

F Hyperparameters

Table 3: Experiment configurations used in this work.

	MNIST	Fashion-MNIST
Architecture		
arch		DiT-S/2
input size		$28 \times 28 \times 1$
patch size		2×2
hidden dim		384
depth		12
register tokens		8
style embedding tokens		32
Optimizer		
optimizer		AdamW ($\beta_1 = 0.95, \beta_2 = 0.999$)
learning rate		$2e-4$
weight decay		$1e-4$
cosine annealing		Yes
warmup steps		300
gradient clip		2.0
training steps	12000	16000
Loss		
class labels N_c		5
positive samples N_{pos}		96
generated samples N_{neg}		96
effective batch $B (N_c \times N_{neg})$		480
kernel widths	{0.025, 0.05, 0.1, 0.15, 0.2, 0.25, 0.3, 0.35, 0.4, 0.5, 1.0}	